Forest Ecology and Management 518 (2022) 120258

Contents lists available at ScienceDirect

Forest Ecology and Management

journal homepage: www.elsevier.com/locate/foreco

Mass fire behavior created by extensive tree mortality and high tree density not predicted by operational fire behavior models in the southern Sierra Nevada

Scott L. Stephens [a,1,*], Alexis A. Bernal [a,1], Brandon M. Collins [a,b], Mark A. Finney [c], Chris Lautenberger [d], David Saah [e,f]

[a] Department of Environmental Science, Policy and Management, 130 Mulford Hall, University of California, Berkeley, CA 94720, USA
[b] Center for Fire Research and Outreach, University of California, Berkeley, CA 94720, USA
[c] USDA Forest Service, Rocky Mountain Research Station, Missoula, Montana 59808, USA
[d] Reax Engineering, 1921 University Ave, Berkeley, CA 94704, USA
[e] Spatial Informatics Group, LLC, Pleasanton, CA 94566, USA
[f] Geospatial Analysis Lab, University of San Francisco, San Francisco, CA 94117, USA

ARTICLE INFO

Keywords:
Creek fire
Restoration
Mixed conifer forest
Wildfire
Drought
Bark beetles

ABSTRACT

Large, severe wildfires continue to burn in frequent-fire adapted forests but the mechanisms that contribute to them and their predictability are important questions. Using a combination of ground based and remotely sensed data we analyzed the behavior and patterns of the 2020 Creek Fire where drought and bark beetles had previously created substantial levels of tree mortality in the southern Sierra Nevada. We found that dead biomass and live tree densities were the most important variables predicting fire severity; high severity fire encompassed 41% of the area and the largest high severity patch (19,592 ha) comprised 13% of total area burned. Areas with the highest amounts of dead biomass and live tree densities were also positively related to high severity fire patch size indicating that larger, more homogenous conditions of this forest characteristic resulted in adverse, landscape-scale fire effects. The first two days of the Creek Fire were abnormally hot and dry but weather during the days of the greatest fire growth was largely within the normal range of variation for that time of year with one day with lower windspeeds. From September 5 to 8th the fire burned almost 50% of its entire area and fire intensity patterns inferred from remotely sensed brightness-temperature data were typical except on September 6th when heat increased towards the interior of the fire. Not only was the greatest heat concentrated away from the fire perimeter, but a significant amount of heat was still being generated within the fire perimeter from the previous day. This is a classic pattern for a mass fire and the high amount of dead biomass created from the drought and bark beetles along with high live tree densities were critical factors in developing mass fire behavior. Operational fire behavior models were not able to predict this behavior largely because they do not include post-frontal combustion and fire-atmosphere interactions. An important question regarding this mass fire is if the tree mortality event that preceded it could have been avoided or reduced or was it within the natural range of variation for these forests? We found that the mortality episode was outside of historical analogs and was exacerbated by past management decisions. The Creek Fire shows us how vulnerable of our current frequent-fire forest conditions are to suffering high tree mortality and offering fuel conditions capable of generating mass fires from which future forest recovery is questionable because of type conversion and probable reoccurring high severity fire.

* Corresponding author.
E-mail address: sstephens@berkeley.edu (S.L. Stephens).
[1] These authors contributed equally to this work.

https://doi.org/10.1016/j.foreco.2022.120258
Received 4 March 2022; Received in revised form 21 April 2022; Accepted 26 April 2022
Available online 16 May 2022

1. Introduction

Fire is an integral component of most western US forests but more than a century of logging and attempted fire exclusion has dramatically changed frequent-fire forests (forests that used to burn every 35 years or less) by increasing tree densities, lowering average tree size, increasing the dominance of shade tolerant species, and increasing fuel loads (Safford and Stevens, 2017; Hagmann et al., 2021; Bernal et al., 2022). Wildfires burning in these forest conditions have increased in size and severity since the late 20th century (Miller et al., 2009; Stevens et al., 2017) with climate change also being a factor (Abatzoglou and Williams, 2016; Westerling, 2016). In addition to altered forests and climate change, recent drought/bark beetle induced tree mortality can also be a factor contributing to exacerbated wildfire behavior and effects (Stephens et al., 2018). An important consideration with large-scale tree mortality is the potential to add long-burning, high fuel loads over extensive areas—fuel characteristics that match the criteria for mass fires. Mass fires (Finney and McAllister, 2011) can occur when large, continuous areas (several km^2) are burning with high intensity for long durations (hours) as seen from multiple earthquake-related ignitions in urban areas and by incendiary bombing in war (Pitts, 1991). Mass fire behaviors result from the strong coupling between the fire and induced atmospheric circulations.

Wildland fire behavior concerns the spread and energy release of free-burning vegetation but is complicated to predict. Modeling of fire behavior is traditionally focused on the characteristics of the flaming edge – its spread rate and fireline intensity as a direct function of fuel, weather, and topographic factors. All US operational fire behavior prediction models are empirical, i.e., based on fitting of experimental data, and suffer from two principal limitations. First, feedbacks between the fire and its environment are not explicitly included, and second, heat release from combustion is restricted to only the short-lived flaming phase of fine fuel materials. Both of these limiting factors are interconnected because heat release over extensive areas (not thin flame zones) from all phases of combustion (flaming and non-flaming) can become coupled with atmospheric circulations that in-turn affect broad-scale fire behaviors for long periods.

In most natural fuel configurations, fine fuel materials (<7.5 cm thick) have a short flaming time, typically varying from a few seconds for grass to perhaps a minute or two for small woody fuel particles (Nelson, 2003). Once flaming has ceased, burning of residual char (often called solid phase combustion) is not modeled but may constitute 30% of the pre-burn fuel mass (Di Blasi et al., 2001), and even a greater fraction of potential residual heat because of its high carbon content (Babrauskas, 2006). Furthermore, combustion characteristics of large woody fuel (logs) and deep organic layers (duff) are completely neglected by current operational models but burn in widely varying fashion – ranging from little consumption, to long-duration smoldering with slow heat release rates, to flaming at high heat release rates. Environmental conditions at the time of burning, including those induced by the fire itself, have a strong influence on the type of combustion and heat release rates in these fuels. One of the most salient fire-induced influences is local winds that effectively ventilate combustion of the long-burning materials. Thus, disparity between predicted and observed fire growth would be expected in fuel types with large or deep fuel materials that support deep combustion zones and long duration burning, occurring well beyond the passage of the flaming edge.

Fuel conditions across vast areas of western US frequent-fire forests are now characterized by high concentrations of large woody material and deep organic layers on the forest floor because the historical regime of frequent fire has been disrupted by fire suppression and exclusion (Hagmann et al., 2021). Burning of these fuel complexes under wildfire conditions may exhibit many of the fire behaviors that are outside the range of modeling capabilities. Key indicators of such fires would be the deep zones of combustion covering large areas for long durations. Such fires could develop pyrocumulonimbus clouds towering to altitudes of 10,000 m (Peterson et al., 2017) (Fig. 1), associated precipitation and downdrafts, and likely vorticity near the ground that further affects burning behaviors of the fuel complex in ways beyond the assumptions and capabilities of operational fire behavior models (Finney et al., 2021).

The overall goal of this project is to investigate extreme fire behavior and effects for a wildfire that occurred in an area affected by high tree mortality prior to the wildfire. We hypothesized that this pre-fire mortality influenced the burning characteristics of the fire itself, as indicated by Goodwin et al. (2021), which may not be captured by current operational fire spread models. We integrated disparate spatial datasets in a novel analytical approach to address the following objectives: (1) quantify the extent and magnitude of tree mortality that preceded the 2020 Creek Fire, (2) use a network of weather data collected before and during this fire to evaluate fire growth with local weather, and (3) predict the fire behavior and severity of the Creek Fire and compared it to its actual behavior. The overall goal of addressing these objectives is to understand drivers of extreme fire behavior in a relatively unique, but likely increasing, forest fuel condition and to assess the potential for current operational fire spread models to capture this behavior (see Fig. 2).

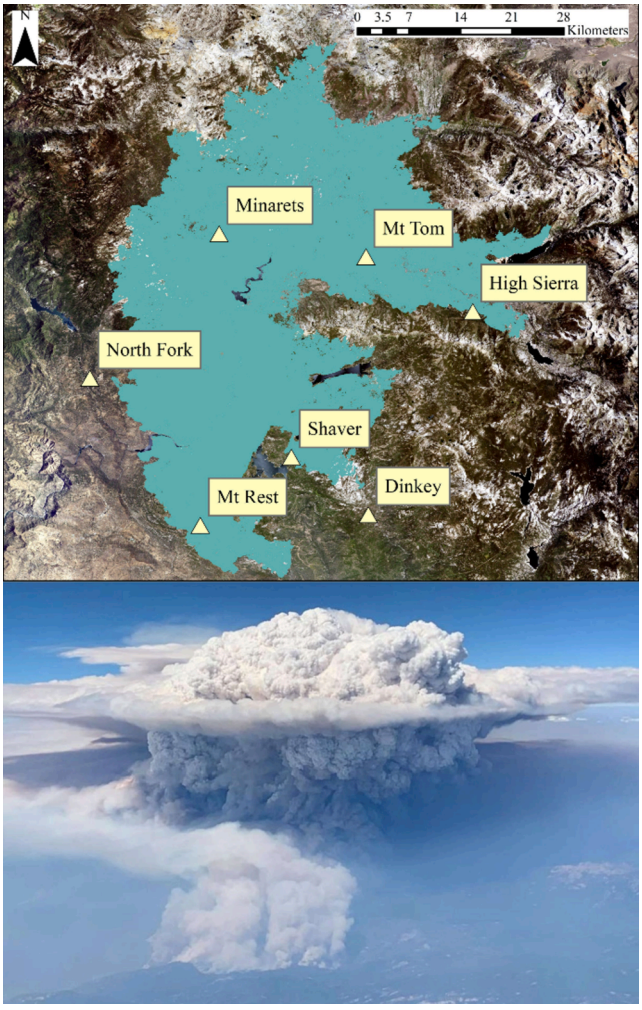

Fig. 1. Locations (triangles) and names of RAWS stations used to create baseline and Creek Fire weather conditions (top panel). Shaded teal area delineates the Creek Fire footprint and is superimposed on aerial photos provided by United States Department of Agriculture National Agriculture Imagery Program (2020). Bottom panel is a photograph of the plume created by the Creek Fire taken by Thalia Dockery.

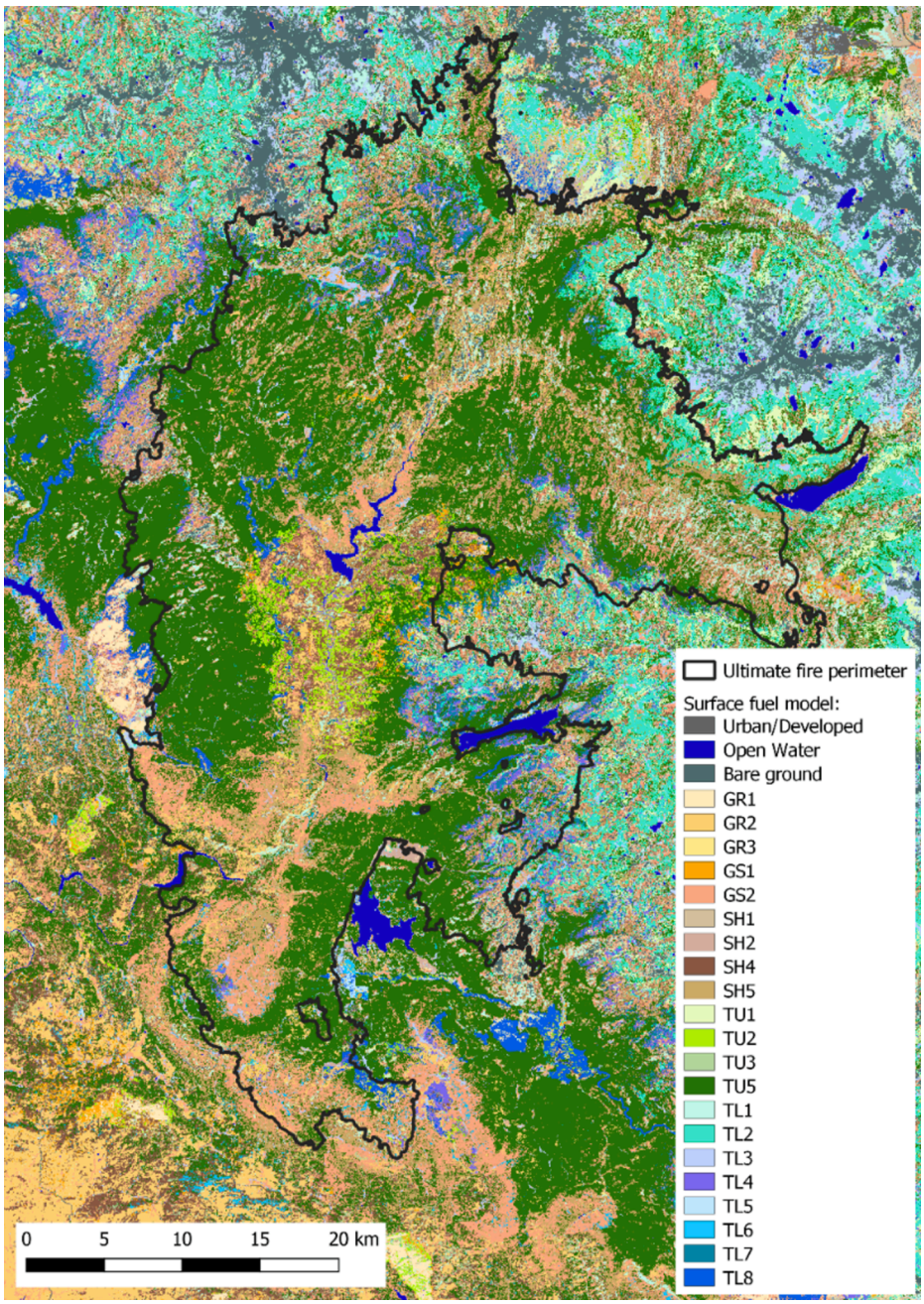

Fig. 2. Map of surface fuel models within the Creek Fire footprint (outlined in black).

2. Materials and methods

2.1. Study site

The Creek Fire burned in the southern Sierra Nevada mostly in the US Forest Service Sierra National Forest (Lat 37° 12′ 4″ Long 119° 16′ 18″). The fire burned 154,000 ha, which began in the early evening on September 4, 2020, in the Big Creek drainage between Shaver Lake and Huntington Lakes, California. The fire burned mostly in mixed conifer forests composed of ponderosa pine (*Pinus ponderosa*), sugar pine (*Pinus lambertiana*), white fir (*Abies concolor*), incense-cedar (*Calocedrus decurrens*), and California black oak (*Quercus kelloggii*). Prior to 1900, low- to moderate-severity fire ignited by lighting and Indigenous communities was common across this area, with mean fire return intervals ranging from 5 to 20 years (Kilgore and Taylor, 1979; Caprio and Swetnam, 1993; Krasnow et al., 2017; Long et al., 2017,2021). This area of the southern Sierra Nevada has varied land-use practices including past wildfires, harvesting operations, recreation, and a limited amount of prescribed fire and other fuel treatments. The Creek Fire is one of the largest forest wildfires in modern California history.

2.2. Fire weather

We collected data from 7 Remote Automated Weather Stations in and around the Creek Fire footprint (Fig. 1) using the Program for Climate, Ecosystem, and Fire Applications and Fire and Aviation Application Information portals. For each station, we collected dry bulb temperature (°C), relative humidity (%), and windspeed (km h^{-1}) from 2000 to 2020, specifically focusing on the common wildfire months of August–October. Station data were then processed within Fire Family Plus to extract hourly weather data for each day as well as hourly fire danger metrics including the energy release component (ERC) and burning

index (BI). ERC reflects the available energy per unit area within the flaming front, and by keeping fuel type constant, becomes an index of changing fuel moisture content. BI is related to the flame length (Bradshaw et al., 1983) and thus a product of both ERC and the fire rate of spread which is heavily influenced by wind speed. These indices from the National Fire Danger Rating System are derived from the Rothermel fire spread equation (Rothermel, 1972) for fuel model "G" which contains four fuel size classes but applies only to fire behavior of a thin flaming front. Both metrics are positively related to fire severity (Lydersen et al., 2014, 2017). For each day, we averaged hourly weather data from 18:00 to 1:00 UTC (11:00–18:00 PST), which is when we expect weather to have the greatest influence on fire behavior.

2.3. Fire growth and intensity

To discern how fire spread and intensity varied with weather, we used the Visible Infrared Imaging Radiometer Suite (VIIRS) aboard the Joint Polar Satellite System (JPSS-1), which provides a 375-m resolution active fire product from the Fire Information for Resource Management System. From this point dataset, we interpolated daily Creek Fire perimeters similar to Briones-Herrera et al. (2020). Based on their methods, we aggregated points for each day of the Creek Fire in R (R Core Team 2020) at 1125 m, with a minimum of 3 points to be considered as part of the daily fire perimeter. Daily aggregated points were then applied with a convex hull algorithm using the *sf* package (Pebesma, 2018) to delineate fire perimeters. When two or more interpolated perimeters overlapped spatially and temporally, we combined those perimeters together. We also created maps of daily fire intensity by converting the VIIRS points into a 375-m resolution raster dataset. To do this, we estimated the Normalized Difference Brightness Temperature Index (NDBTI: Eq. (1)):

$$NDBTI = \frac{T4 - T5}{T4 + T5} \quad (1)$$

where T4 and T5 represent the brightness temperature (Kelvin) of the VIIRS I4 and I5 bands, respectively (Waigl et al., 2017). Both bands are used in the active fire detection and characterization algorithm, with I4 used as the predominant band for active fire detection and I5 used to compliment I4 by correcting saturated pixels. Elevated NDBTI values indicate higher fire intensity, which can distinguish active fire fronts from residual fire within a fire perimeter (Waigl et al., 2017). However, cases can arise where I4 < I5, resulting in a negative NDBTI value. This anomalous condition is an artifact of pixel saturation due to the low temperature threshold of the I4 band (367 K). In these cases, pixels were assigned a value equivalent to the maximum NDBTI value for a given day to better represent those pixels displaying high fire intensity.

2.4. Fire severity

Fire severity was estimated according to corrected methods established by Parks et al. (2018), which uses the Google Earth Engine platform to derive Landsat-based fire severity indices. We created a 30 m resolution raster of an extended assessment of the relativized delta normalized burn ratio (RdNBR) using Landsat imagery from the year prior to and after the start date of the Creek Fire (September 4, 2020). We then categorized RdNBR values into four fire severity classes (unchanged, low, moderate, and high) based on thresholds for the composite burn index described by Miller and Thode (2007).

2.5. Forest structure and composition

To quantify forest structure following drought and bark beetle attacks (2012–2016) in the southern Sierra Nevada, we used live tree density (trees ha^{-1}) and live tree basal area (m^2 ha^{-1}) from F3. F3 is a 30-m resolution raster dataset that integrates Forest Inventory and Analysis data and uses the Forest Vegetation Simulator (FVS) to model initial stand conditions and project succession over time (Huang et al., 2018). It then uses Field and Satellite for Ecosystem Mapping to incrorporate remotely-sensed data (Light Detection and Ranging data and Landsat imagery) to simulate spatiotemporal forest patterns across larger scales. Since tree mortality data were not available for F3, we used the change in live basal area from 2011 to 2016 to estimate the amount of snag basal area generated during the drought and bark beetle attacks. However, this approach means that mortality is only detectable if there was a decrease in basal area from 2011 to 2016. Predicted tree mortality between 2011 and 2016 is mainly driven by a stand density index-based mortality model within FVS which applies either background or density-dependent mortality rates when relative stand density index is below or above a minimum threshold, respectively (Dixon et al., 2008). F3 uses regionally-specific mortality models developed for FVS variants (Huang et al., 2018), with the western Sierra Nevada variant accounting for basal area distribution and species to estimate mortality rates for individual trees (Dixon et al., 2008). However, this approach mainly attributes mortality among smaller-sized trees without consideration for the spatially interactive processes that govern the species and size of trees that die following large-scale disturbances (Huang et al., 2019). Given that the region encompassing the Creek Fire footprint suffered the greatest mortality among large ponderosa pine that likely died from bark beetle-associated mortality (Fettig et al., 2019), our estimates of mortality and fuels generated by that mortality may be lower than what existed in this region prior to the Creek Fire.We converted snag basal area to a percent of total basal area within a given pixel. We also converted snag basal area to dead biomass (Mg ha^{-1}) using aboveground biomass allometric equations provided by Knight et al. (2020) to estimate dead fuels that were available to burn during the Creek Fire.

2.6. Previous fire history

Since previous wildfire activity can influence subsequent fire behavior and effects (Lydersen et al., 2019), we accounted for wildfire history within the Creek Fire footprint. Wildfire data from 1984 to 2017 were obtained from Miller (2017), which included all wildfires >81 ha in size. Although this window omits three years prior to the Creek Fire, there were no additional wildfires within the Creek Fire footprint from 2017 to 2020, totaling 23 wildfires prior to the Creek Fire. We converted fire perimeter polygons to a 30-m resolution raster dataset, with pixel values ranging from 0 to 3 indicating the number of times burned.

2.7. Previous treatment history and topography

Fuel reduction and forest restoration treatments can have an impact on fire behavior and effects (Stephens et al., 2009). We accounted for treatment history within the Creek Fire footprint by using the US Forest Service Activity Tracking System (FACTS), which contains a database of polygons delineating various treatments that are planned or completed. These treatments included fire hazard reduction, range improvement, reforestation, timber stand improvement, and timber harvesting. We chose to only include treatments that were completed from 2011 until the start date of the Creek Fire to evaluate how treatments implemented during the drought and bark beetle attacks may have impacted the Creek Fire. We converted polygons to a 30-m resolution raster dataset, with pixel values categorized as 0 or 1 to indicate the absence of presence of treatments, respectively.

Topographic data were acquired from LANDFIRE and included elevation (m), slope (degrees), and aspect (degrees). We converted aspect to a categorical variable with breakpoints at 0°/360°, 90°, 180°, and 270° to correspond to northeast-facing, southeast-facing, southwest-facing, and northwest-facing slopes, respectively. All spatial data including forest structure and composition, previous fire history, previous treatment history, and topography were cropped and aligned with the extent of the fire severity raster we generated (~30 m resolution;

World Geodetic System 84).

2.8. Modeled fire behavior

The operational fire spread model ELMFIRE (Lautenberger, 2013, 2017) was used to model initial progression of the Creek Fire from September 4 to 8, 2020 under conventional modeling assumptions that could have realistically been applied for real-time forecasting. ELMFIRE can be thought of as a gridded ensemble implementation of 2D Rothermel-based fire models such as FARSITE (Finney, 1998) with some differences in how the fire front is tracked and crown fire and spotting are estimated. ELMFIRE is uncoupled to the atmosphere. Although the Creek Fire's specific origin area and time of ignition are not precisely known, (per Inciweb: National Wildfire Coordinating Group, 2020a) the ignition coordinates are taken as (−119.272°, 37.201°) with an ignition time of 18:30 PDT on September 4th. Fire model inputs were specified as follows:

- Topography and surface/canopy fuels: Pyrologix' 2020 California Fuelscape data that are based on LANDFIRE 2016 Remap 2.0.0 (LF Remap). Calibration workshops with interagency fire and fuels personnel were held to develop a calibrated fuelscape that produces locally accurate fire behavior results. Since LF Remap does not included disturbances after 2016, spatial data on fuel disturbances (fire, fuel treatments, mortality, etc.) through early 2020 were then incorporated into the fuelscape to provide a fuelscape suitable for use in California during the 2020 fire season. Additional details are provided in Brough et al. (2020).Wind speed and direction, relative humidity, and temperature: Real Time Mesoscale Analysis (National Oceanic and Atmospheric Administration, 2020) which provides hourly estimates of sensible weather variables on a 2.5 km grid for the Continental US
- Dead fuel moisture: Calculated from gridded Real Time Mesoscale Analysis data using NFDRS procedures (Bradshaw et al., 1983)
- Live fuel moisture: Estimated from national fuel moisture database (United States Forest Service, 2020)

ELMFIRE was run in a 1000-member ensemble with wind speed perturbed at ±3 mph, wind direction perturbed at ±15°, spread rate adjustment factor varied from 0.8 to 1.2, and dead fuel moisture content perturbed by ±0.01%. Fire perimeter snapshots were extracted from the 90th percentile ensemble member. The modeled growth of the Creek Fire was then compared to the actual fire perimeters to evaluate how well ELMFIRE predicted this event.

2.9. Data analysis

To evaluate how weather conditions during the Creek Fire compared to average weather conditions for the region, we measured the departure of weather conditions from the year the Creek Fire burned relative to previous years. To do this, we used the *boot* package in R (Canty and Ripley, 2017) to bootstrap 95% confidence intervals (1000 permutations) for each daily weather metric across all weather stations (Fig. 1) from 2000 to 2019 to establish a baseline of average weather conditions for the region. When then bootstrapped 95% confidence intervals across all weather stations for 2020 and compared if daily weather conditions during the Creek Fire overlapped with our baseline. We then compared fire weather days with the days of greatest fire spread and intensity during the Creek Fire.

To determine if prior forest conditions influenced fire severity, we used the *rpart* package in R (Therneau and Atkinson, 2019) to create a categorical regression tree that identified environmental thresholds that were associated with Creek Fire severity. We extracted values of live tree density, percent basal area of snags, fuels (i.e., dead biomass), previous fire history, previous treatment history, and topography from our raster datasets using a 180-m grid of points across the Creek Fire footprint. A spacing of 180 m was chosen to minimize biases that arise from spatial autocorrelation associated with modeling fire severity (Kane et al., 2015). This resulted in a sample size of 47,680 points. With those extracted values as explanatory variables to predict fire severity, we used a class method for splitting variables and a complexity parameter of 0.01 (the increase in R^2 value at each split that must occur for the split to be accepted).

Since environmental conditions within an individual pixel insufficiently captures the spatial context in the surrounding area, which can be quite influential for fire effects (Povak et al., 2020), we used the *patchwoRk* package in R (Sanchez, 2019) to evaluate whether prior forest conditions at larger scales influenced the fire severity patterns observed during the Creek Fire. To characterize landscape-scale, high severity patterns within the Creek Fire footprint, we delineated patches of high severity using the PatchMorph tool (Girvetz and Greco, 2007; Sánchez Meador, 2019). This algorithm determines the size and shape of patches by specifying minimum patch width and maximum width of gaps within a patch. Similar to studies that used this tool to delineate patches of fire severity, we used a minimum patch width and maximum gap thickness of 90 m (or three 30-m pixels) and a minimum patch size of 0.5 ha (Collins and Stephens, 2010, Stevens et al., 2021). Using our regression tree model, we created a continuous map of pre-fire forest conditions across the entirety of the Creek Fire footprint and used the thresholds identified to aggregate patches of forest conditions (now referred to as forest condition departure classes; FCD) using the PatchMorph tool. We used the same patch constraints delineating high severity fire patches. We extracted the percent area from patches of FCD that intersected with high severity fire patches and used a log-transformed linear model to evaluate how the scale of FCD may have influenced high severity fire patch size.

3. Results

Baseline conditions from 2000 to 2019 from our weather station network (Fig. 1) averaged 19 °C, 38% relative humidity, and 6 km h^{-1} windspeed. Similar conditions were observed in 2020, with average temperature 19 °C, 35% relative humidity, and 5 km h^{-1} windspeed. However, the first two days of the Creek Fire were abnormally hotter and drier (Fig. 3), with temperature 5 °C higher and relative humidity 6% lower than baseline conditions ($p < 0.05$). Windspeed for those same days were within the normal range of variation. Despite initial hotter and drier conditions, we found that all weather metrics during the days of the greatest fire growth (September 6–September 8; Fig. 4) were largely within the normal range of variation for late summer and early autumn except for September 6th that had a lower windspeed. When evaluating metrics of fire danger, we found that the first five days of the Creek Fire, including the period of highest spread, were within the normal range of variation for both ERC and BI ($p < 0.05$; Fig. 5).

From September 5 to September 8, the fire burned almost 50% of the entire Creek Fire footprint. Upon closer examination of these large fire growth days, the spatial distribution of fire intensity revealed some notable patterns (Fig. 6). On September 5th, fire intensity was typical, with heat concentrated on the perimeter of the active flaming front. However, on the largest growth day (September 6), fire intensity was reversed, with heat increasing towards the interior of the fire perimeter. Not only was the greatest heat concentrated away from the fire perimeter, but a significant amount of heat was still being generated within the fire perimeter from the previous day. This pattern reversed back to what we would expect from a typical active flaming front by September 7th, with heat increasing towards the perimeter and heat from previous days subsiding.

Prior to the Creek Fire, we found that the drought and bark beetle attacks from 2012 to 2016 created substantial levels of tree mortality and dead fuels. By 2016, average percent of snag basal area was 37%, with most (63%) of the area characterized by moderate tree mortality (25–75%). Tree mortality translated to an average of 65 Mg ha^{-1} of dead

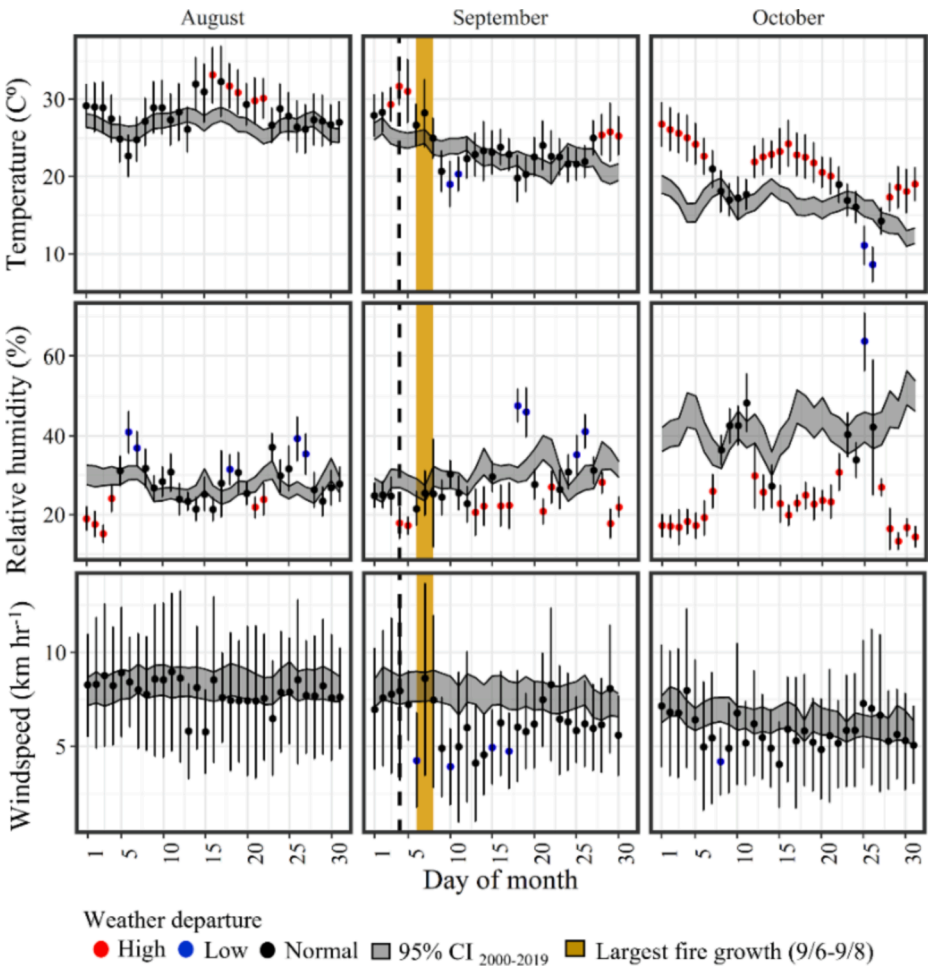

Fig. 3. Creek Fire weather departure from baseline conditions (2000–2019). Gray shaded areas are bootstrapped 95% confidence intervals for baseline weather conditions, while error bars are confidence intervals for 2020. Initiation date of Creek Fire denoted with dashed line and gold shaded area are the days of largest fire spread (September 6–8th). Colored dots represent significant ($p < 0.05$) departure from baseline conditions, with red indicating more severe fire weather, blue indicating lower, and black indicating observation falls within normal range of variation. (For interpretation of the references to colour in this figure legend, the reader is referred to the web version of this article.)

biomass, with the interquartile range spanning 25–92 Mg ha^{-1}. Despite increased levels of tree mortality, live tree density (trees > 2.5 cm diameter-at-breast-height) was still high in 2016, averaging 622 trees ha^{-1}.

Dead biomass and live tree densities were the most important variables in our categorical regression tree analysis predicting fire severity. Dead biomass, in particular, had the strongest influence on pixel-level fire severity (Fig. 7), with > 46 Mg ha^{-1} resulting in high severity. In areas below this level of dead biomass, the lowest tree densities (<232 trees ha^{-1}) were associated with low severity, while the highest tree densities (>693 trees ha^{-1}) at low elevation (<2430 m) were associated with high severity. Intermediate levels of tree density (232–693 trees ha^{-1}) had mixed effects, producing moderate severity at lower elevation (<2430 m) and low severity at higher elevation (>2430 m). Our regression tree did not identify fire history or past forest treatments as factors related to fire severity. We also could not distinguish the contributing factors related to unchanged fire severity due to the small sample size of these observations.

Among fire severity classes, high severity accounted for the greatest proportion of area (41%) burned in the Creek Fire (61,305 ha; Fig. 8), followed by moderate severity (35%; 52,768 ha), low severity (21%; 30,917 ha), and unchanged (3%; 4920 ha). When aggregated as patches ≥ 0.5 ha, we found that that the Creek Fire created very large contiguous areas of high severity, with the largest high severity patch (19,592 ha) comprising 13% of total area burned (Fig. 8). This is a stark contrast compared to the other fire severity strata, where the cumulative area of the largest patches across unchanged, low, and moderate severity only made up 1% of total area burned (245, 699, and 1014 ha, respectively).

We used the thresholds identified in the regression tree analysis to map and analyze three forest condition departure (FCD) classes: FCD-high, FCD-mod, and FCD-low (Table 1). Prior to the Creek Fire, a majority (66%; 99,115 ha) of the landscape was composed of patches in the FCD-high class (dead biomass >46 Mg ha^{-1} and >693 trees ha^{-1}), with the largest patch in this class being 83,645 ha in size. FCD-mod (407–693 trees ha^{-1} and elevation <2430 m or 232–407 trees ha^{-1}) patches accounted for 21% of the landscape, followed by FCD-low (<232 trees ha^{-1} or 407–693 trees ha^{-1} and elevation > 2430 m) patches which represented 9% of the landscape. The distribution of FCD classes within individual patches of high severity (Fig. 9) revealed that FCD-high overwhelmingly burned at high fire severity (91%). While FCD-low and FCD-mod were interspersed in high severity patch areas, they consisted of <31% of total high fire severity area. Our linear model also revealed some notable patterns in the influence of forest conditions on landscape-level, high severity fire effects. Only FCD-high was positively related to high severity fire patch size ($p = 0.029$), indicating that larger, more homogenous conditions of this forest characteristic resulted in adverse, landscape-scale fire effects.

3.1. Fire spread modeling

Modeled fire spread was compared to actual fire growth with cumulative MODIS (National Wildfire Coordinating Group, 2020b), VIIRS (National Wildfire Coordinating Group, 2020c), and IR (National Interagency Fire Center, 2020) fire detections at several discrete times between September 4th and September 8th, 2020 (Fig. 10). Using ELMFIRE, the rapid northward fire growth on September 5th and September 6th was not captured (Fig. 10b and c). The offshore wind event that impacted the region on September 7th and September 8th

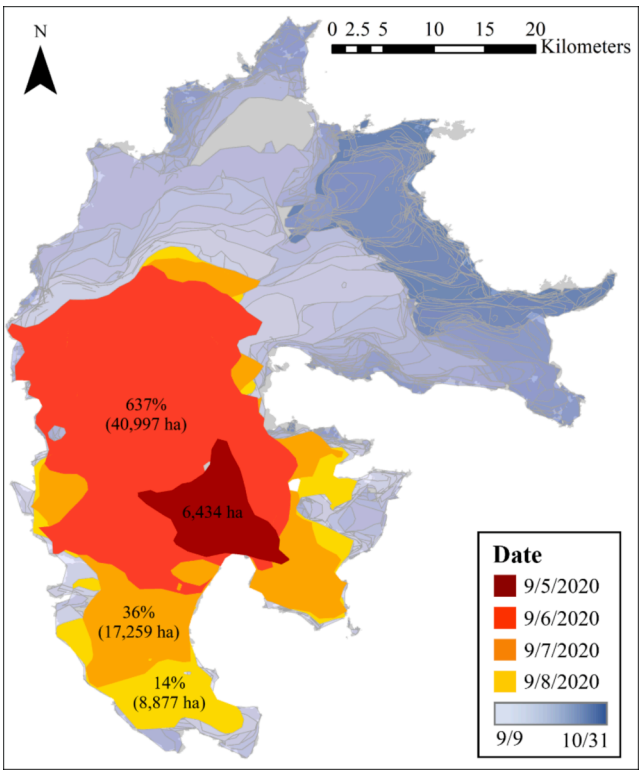

Fig. 4. Creek Fire growth during the days of greatest fire spread. Colored polygons delineate daily fire growth, with percentage of growth relative to previous day indicated. Absolute size of growth (ha) for a given day indicated in parenthesis. The total amount of area burned during the four days of greatest fire spread consisted of almost 50% of the entire Creek Fire footprint. Shaded polygons in blue and outlined in gray delineate fire spread during subsequent days (9/9/2020–10/31/2020). (For interpretation of the references to colour in this figure legend, the reader is referred to the web version of this article.)

drove fire to the southwest. As shown in Fig. 10d and e, this was captured to some degree in the model, with some discrepancies in timing and extent of the run.

4. Discussion

This work identified several factors that contributed to the extreme behavior of the Creek Fire. Before discussing these factors, it should be stressed that the forests within the Creek Fire were already highly altered from fire suppression/exclusion and past harvesting. An extensive 1911 inventory of mixed conifer forests to the southwest of the Creek Fire was compared to contemporary conditions and found drastic differences, particularly in tree density, canopy cover, the density of large trees, and the dominance of white fir that collectively increased fire hazards and reduced forest resilience (Stephens et al., 2015). These conditions alone have led to increased percentages of high severity fire and high severity patch size in the Sierra Nevada (Miller et al., 2009) even without the large-scale tree mortality that happened during the 2012–2016 drought. Increasing burn severity and larger high severity patches is a problem because it can lead to a reduction in frequent-fire forests from type conversion to shrublands or other vegetation types (Coop et al., 2020).

The Creek Fire destroyed at least 853 buildings and cost over $193 million (2020 USD) to suppress (NIFC, 2020). While lightning ignited fires and Indigenous burning have been a part of this landscape for thousands of years (Caprio and Swetnam, 1993; Long et al., 2017,2021; Krasnow et al., 2017), the severity patterns within the Creek Fire are completely outside the historical range of variation of mixed conifer forests (Safford and Stevens, 2017). In similar mixed conifer forests in the Greenhorn Mountains southwest of the Creek Fire, the historic percentage of areas that experienced high severity fire was low and varied from 1% to 3% (Stephens et al., 2015). This is in stark contrast to the Creek Fire that was 41% high severity with the largest single, high severity patch (19,592 ha) comprising 13% of total area burned.

Prior to the Creek Fire, a majority (66%) of the landscape was composed of patches in the FCD-high class. Our analysis revealed that FCD-high areas overwhelmingly burned at high fire severity (91%) during the Creek Fire. Our model also revealed some notable patterns regarding the influence of forest conditions on landscape-level, high

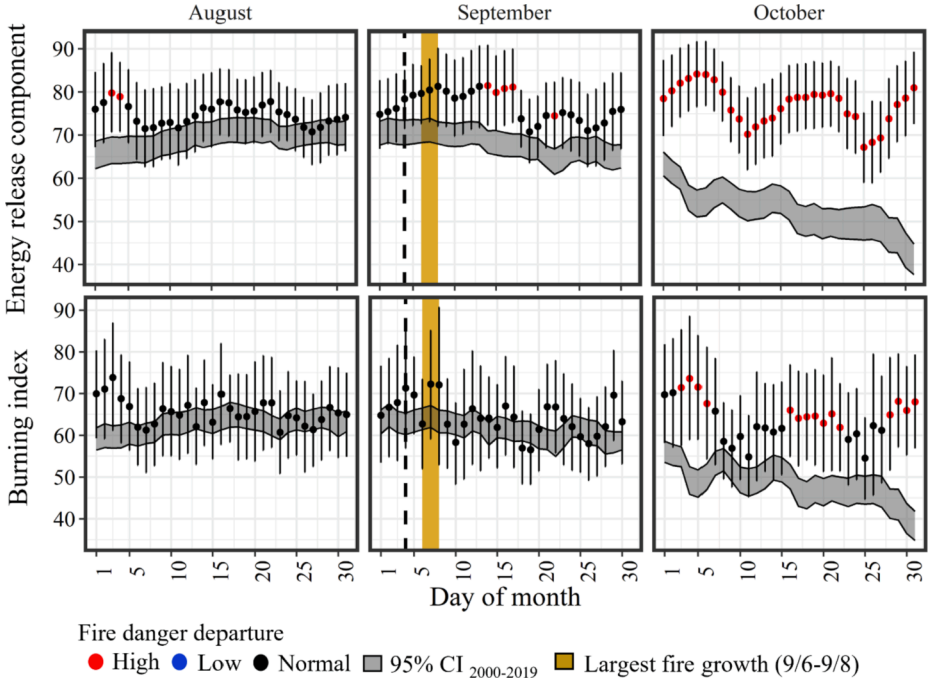

Fig. 5. Creek Fire danger departure from baseline conditions (2000–2019). Gray shaded areas are bootstrapped 95% confidence intervals for baseline fire danger conditions, while error bars are confidence intervals for 2020. Initiation date of Creek Fire denoted with dashed line and gold shaded area are the days of largest fire spread (September 6–8th). Colored dots represent significant ($p < 0.05$) departure from baseline conditions, with red indicating higher fire danger, blue indicating lower, and black indicating observation falls within normal range of variation. (For interpretation of the references to colour in this figure legend, the reader is referred to the web version of this article.)

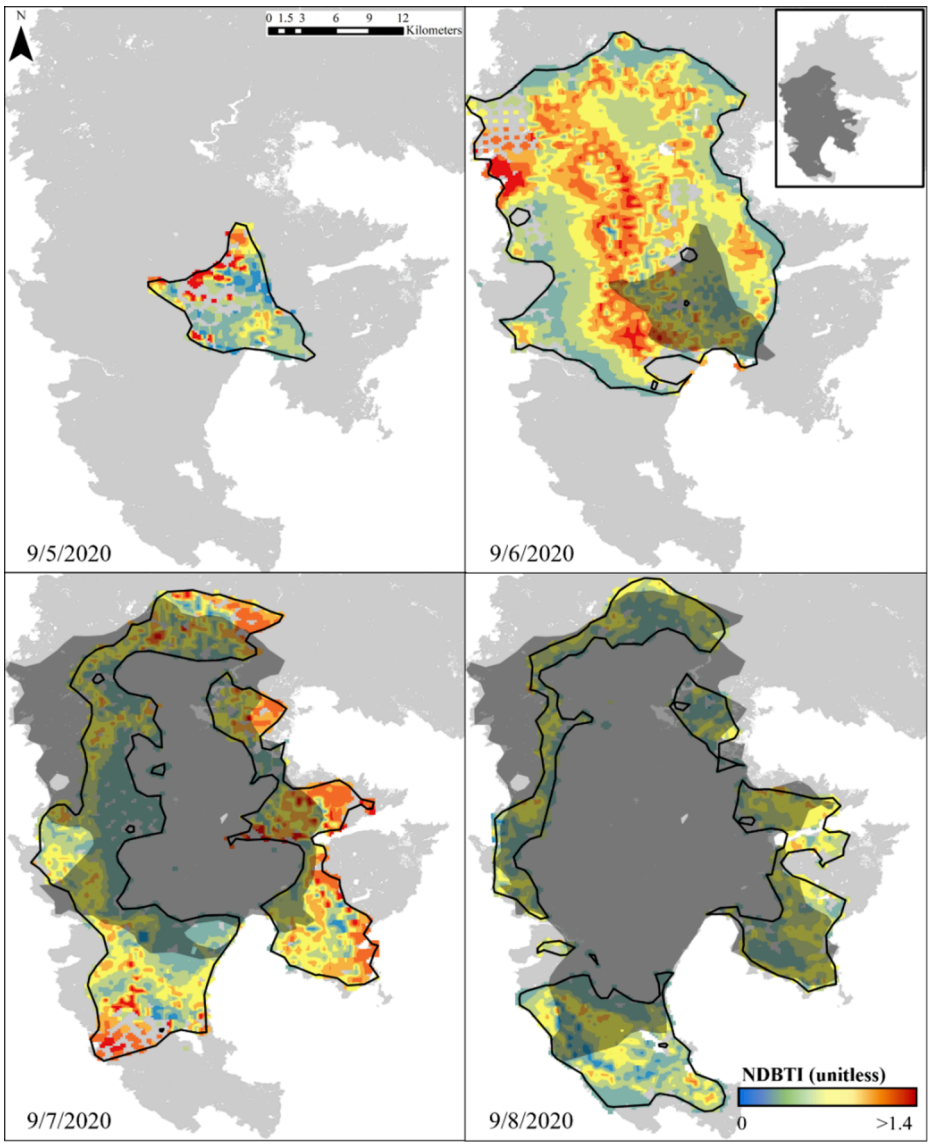

Fig. 6. Distribution of daily fire intensity using the Normalized Difference Brightness Temperature Index (NDBTI), where higher values indicate greater fire intensity. Days that experienced the largest growth relative to the previous day (>10%) are shown. Light gray area delineates the Creek Fire footprint while the dark shaded area delineates the total fire perimeter from previous days. The inset shows the location of the daily fire perimeters relative to the entirety of the Creek Fire footprint.

severity fire effects. Only FCD-high was positively related to high severity fire patch size ($p = 0.029$), indicating that larger, homogenous FCD-high conditions resulted in adverse, landscape-scale fire effects. Indeed, the condition of this forest prior to and after the 2012–2016 drought contributed to the behavior and effects of the Creek Fire. This assertion is also supported by the findings Goodwin et al. (2021), which demonstrated considerably greater potential energy release from wildfire following drought-related tree mortality. If drought and bark beetle induced mortality occurs in other areas of the Sierra Nevada (i.e. the northern Sierra Nevada) or elsewhere, we expect that similar fire effects could be produced.

This research found that the largest factors that contributed to high severity fire within the Creek Fire were dead biomass and live tree densities. Dead biomass, in particular, had the strongest influence on pixel-level fire severity (Fig. 7). Although the first two days of the Creek Fire were abnormally hotter and drier, all weather metrics during the days of the greatest fire growth (September 6–September 8) were largely within normal ranges (except September 6th that had lower windspeeds, the day the fire grew the most). More evidence regarding fire weather is provided by the National Fire Danger indices: on September 6th the fire grew 637% (40,997 ha) relative to the previous day although BI and ERC were within normal range of variation (Figs. 3 and 5). This is an important result that provides further evidence that the fire behavior during its more severe burning periods did not conform to the standard line-fire modeling assumptions but was instead a function of more complex interactions of fuel and fire-induced atmospheric conditions. This strong fuels signal in the severity the Creek Fire was also corroborated by an analysis of all large 2020 wildfires in California (Safford et al., 2022), which also identified the nearby 2020 Castle Fire as having a similar fuels-dominated signal.

High rates of energy release over large areas are the preconditions for fire behaviors called firestorms or mass fires (Carrier et al., 1981,1985) that become dynamically dependent upon strong atmospheric interactions. The strong coupling between the fire and atmosphere means that fire growth and behaviors along any portion of the burning area are themselves a function of large scale fire-induced atmospheric flows such as strong downdrafts, indrafts, and vorticity of the entire plume or lee-side edges. High surface winds and vortices along the fire front loft and transport burning material far from the fire edge and further expand fire growth. Recent analysis of RADAR revealed smoke plumes above the

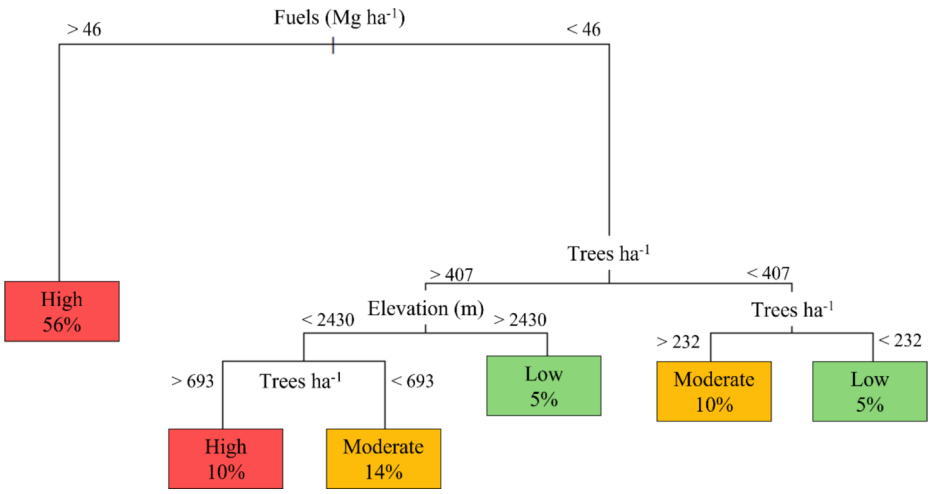

Fig. 7. Regression tree output explaining the influence of environmental conditions on fire severity. Colored boxes at the ends of the regression tree branches contain categories of fire severity (low, moderate, and high) and percentage of observations in each resulting group.

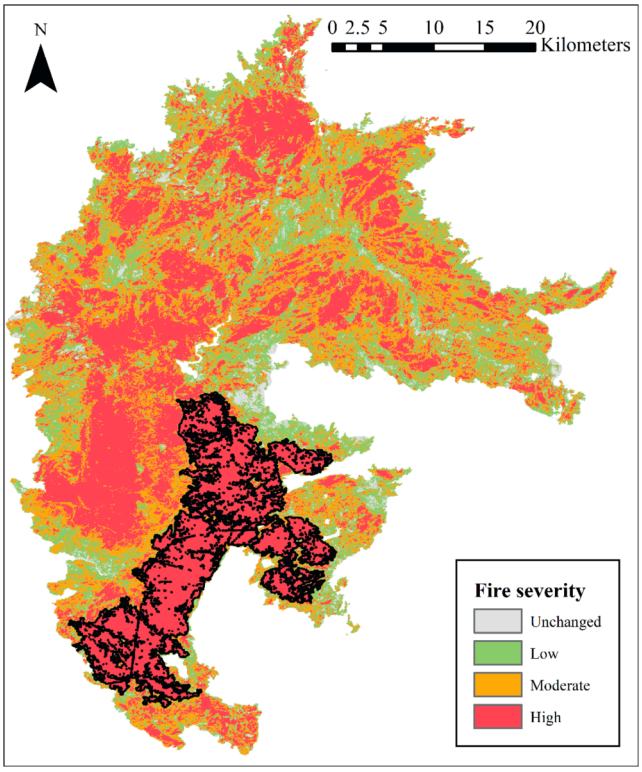

Fig. 8. Map of fire severity according to classes based on composite burn index (CBI) values including unchanged (CBI 0–0.1), low (–0.1-1.25), moderate (1.25–2.25), and high (2.25–3). The high severity patch with black border delineates the largest patch in our dataset (19,592 ha).

Creek Fire and two other large fires in California, contained counter rotating vortex pairs and associated high surface winds along the lee edges of the fire for up to 9 h and 20 km of fire spread (Lareau et al., 2022). Although fuel conditions were not evaluated by Lareau et al. (2022), the observed vorticity would likely have been initiated by prolonged area-wide burning which forces ambient wind flow around the fire front to create vorticity (i.e. Countryman, 1964) rather than a thin flame zone that is penetrated by surface winds. Sustaining the plume and vorticity would then be aided by long-duration heat release from heavy fuels across large areas, some of which would be remote from the outer fire edge as observed here. The high rates of energy release across the

Table 1
Description of forest condition departure classes (FCD) determined by thresholds found for fuels, tree density, and elevation using categorical regression tree analysis.

Class	Fuels (Mg ha^{-1})	Trees ha^{-1}	Elevation (m)
FCD-low	<46	<232	All elevations
FCD-low	<46	407–693	>2430
FCD-mod	<46	407–693	<2430
FCD-mod	<46	232–407	All elevations
FCD-high	<46	>693	<2430
FCD-high	>46	All tree densities	All elevations

burning area are themselves enhanced by the strong fire-induced surface winds that ventilate the combustion of solid fuel materials. Thus, the growth and energy release from any portion of these fires becomes dependent on the atmospheric circulations generated by the heat release from the entire fire.

This explanation is consistent with the changes in heat release patterns observed from September 5 to September 8 (Fig. 6). On September 5th, fire intensity was typical for most wildfires with heat concentrated on the fires perimeter. However, on the largest growth day (September 6th), this was pattern was reversed, with heat increasing towards the interior of the fire. Not only was the greatest heat concentrated away from the fire perimeter, but a significant amount of heat was still being generated within the fire perimeter from the previous day (Fig. 6). At the whole-fire scale, prolonged heat release from the interior would sustain the buoyant updrafts in the plume core that interact with the wind, moisture, and temperature profiles of the atmosphere. This is a classic pattern for a mass fire and the high amount of large, dead biomas created from the drought and bark beetle attack along with high tree density (that produced large amounts of crown fuels) were critical factors in developing mass fire behavior as anticipated by Stephens et al. (2018). Severe drought during this period exacerbated by climate change was also a contributing factor because it reduced fuel moistures to even lower levels that further adds to the vulnerability of these forests (Williams et al., 2022).

4.1. *Management implications*

Fire behavior exhibited by the Creek Fire during its initial progression is well outside the capabilities of current-generation fire models. Modeling initial spread of the Creek Fire with any conventional fire model will result in a dramatic under-prediction in spread rate and area burned because these models do not capture the physics that drove the

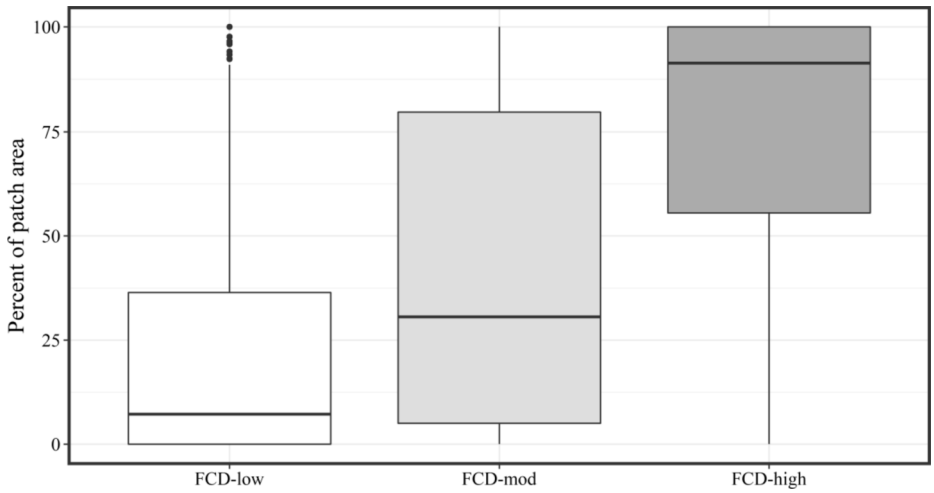

Fig. 9. Percentage of overlap area between forest condition departure classes (FCD) and high severity fire patches.

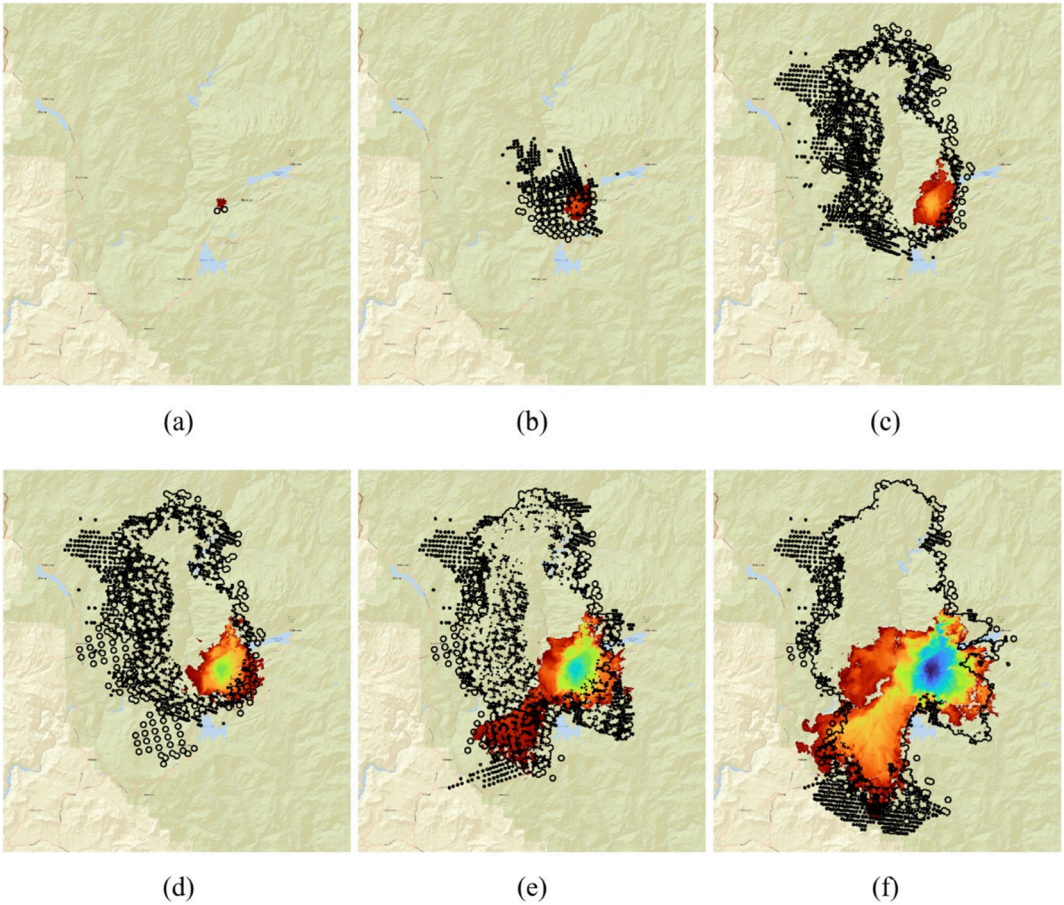

Fig. 10. ELMFIRE modeled progression of the Creek Fire (blue to red contours) compared to observed fire perimeter (black lines) from September 4 to 8, 2020. (a) September 5th 05:50 UTC (b) September 5th 21:42 UTC (c) September 6th 10:50 UTC (d) September 7th 05:33 UTC (e) September 7th 21:36 UTC (f) September 8th 21:40 UTC. (For interpretation of the references to colour in this figure legend, the reader is referred to the web version of this article.)

Creek Fire's initial spread including post-frontal combustion and fire-atmosphere interactions. This outcome is particularly challenging to managers who always prioritize firefighter and public safety. With no operational fire model able to predict such an event, managers can easily underrepresent such events, particularly in areas that experienced considerable tree mortality. It should be noted, however, that extreme fire behavior associated with plume-dominated fire spread is not limited to areas with extensive pre-fire tree mortality (Povak et al., 2020). The potential for extreme fire behavior to cause great harm to human life was demonstrated when the Creek Fire necessitated the rescue of people by National Guard helicopters. The fire trapped visitors at Mammoth Pool Reservoir after it jumped the San Joaquin River and the US National Guard rescued >100 people from this location.

An important question regarding mass fire behavior exhibited by the

Creek Fire is whether the tree mortality event that preceded it could have been avoided or reduced in intensity or was it within the natural range of variation for these forests? To help answer this question we can learn from a severe drought that impacted the forests in southern California and northern Baja California from 1999 to 2002 (Minnich et al., 2016). This severe drought and bark beetle attack killed millions of trees in mixed conifer and pine dominated forests in the San Bernardino and Cleveland National Forests in the US but had a very different impact on Jeffrey pine (*Pinus jeffreyi*)-mixed conifer forests in the Sierra San Pedro Matrir (SSPM) in northern Baja California, Mexico (Stephens and Fule, 2005). Both of these forests are in the Peninsular Mountains with similar soils, topography, climate, past fire frequency, and tree species but the SSPM does not have any ponderosa pine but includes all other mixed conifer tree species (Stephens et al., 2003; Stephens and Gill, 2005; Dunbar-Irwin and Safford, 2016). Although these forests are similar ecologically their management histories are very different with the SSPM never being harvested and fire suppression beginning in 1970, versus on the US side of the border, extensive harvesting occurred along with 120 years of fire exclusion and suppression (Dunbar-Irwin and Safford, 2016; Rivera-Huerta et al., 2016).

In 1932 mixed Jeffrey pine forests in the San Bernardino Mountains had an average density of 95 trees ha^{-1} (trees > 12.5 cm dbh) (Minnich et al., 1995); current tree density from the SSPM for trees > 10 cm dbh is 110 trees ha^{-1} which is similar to that reported in the San Bernardino Mountains before large-scale fire suppression or harvesting (Stephens and Fule, 2005). In 1992, mixed Jeffrey pine forests in the San Bernardino Mountains had tree densities 79% larger than those in the early 1930s mainly because of fire suppression (Minnich et al., 1995). This dramatic change in forest density shaped the drought/bark beetle responses from these areas. Drought and bark beetle mortality (1999–2002) increased snag density in the SSPM by approximately 1.0 snag ha^{-1} to an average of 5 ha^{-1} (Stephens, 2004) but in southern California forests, snag density increased to 125 snags ha^{-1} in many areas (Sims, 2004; Stephens and Fule, 2005).

Past forest management on the US side of the Peninsular Mountains predisposed these forests to a massive tree die-back but on the Mexican side of the border, the forests were able to incorporate these stresses with only modest mortality. Neither Californian tree mortality event (1999–2002 southern California or 2012–2016 southern Sierra Nevada) have historical analogs. Further evidence of the vulnerability of Sierra Nevada mixed conifer forests to severe mortality is provided by a recent study that found historic forests experienced very little competition versus today when 82–95% of mixed conifer forests are in the full occupancy or imminent mortality classes (North et al., 2022). When Sierra Nevada forests were subjected to drought and increased heat stress from climate change, tree defenses were compromised and millions of trees died but the resilient forests in the SSPM persisted (Stephens and Fule, 2005; Stephens and Gill, 2005).

Amazingly, when SSPM Jeffrey pine-mixed conifer forests burned in a wildfire the year after a severe drought ended (2003), the combination of drought/bark beetles and wildfire only killed 20% of the trees and the forest remains in a resilient condition today (Murphy et al., 2021). The good news is California mixed conifer and other frequent-fire adapted forests can become more resilient if we undertake forest restoration (Stephens et al., 2021) at the necessary scales (North et al., 2012; Hessburg et al., 2021; Prichard et al., 2021) and intensity (North et al., 2021,2022). The 2020 Creek Fire shows us how vulnerable our current forest conditions are to suffering high tree mortality and offering fuel conditions capable of generating firestorms and mass fires from which future forest recovery is questionable.

Declaration of Competing Interest

The authors declare that they have no known competing financial interests or personal relationships that could have appeared to influence the work reported in this paper.

Acknowledgement

We thank John Battles and Danny Foster for discussions related to this project and Chuck McHugh for assisting with the Fire Danger Rating System analysis. We also thank Zack Steel for helping to generate the fire severity spatial layer for the Creek Fire. This study was funded by the California Energy Commission's Eletrical Program Investment Charge Program (Grant# EPC-18-026). It does not nesessarily represent the views of the Energy Commission, its empoyees, or the State of California.

References

Abatzoglou, J.T., Williams, A.P., 2016. Impact of anthropogenic climate change on wildfire across western US forests Proc. Nat. Acad. Sci. 113, 11770–11775.
Babrauskas, V., 2006. Effective heat of combustion for flaming combustion of conifers. Can. J. For. Res. 36 (3), 659–663.
Bernal, A.A., Stephens, S.L., Collins, B.M., Battles, J.J., 2022. Biomass stocks in California's fire-prone forests: mismatch in ecology and policy. Env. Res. Let. 17 (4), 044047.
Bradshaw, L.S., Deeming, J.E., Burgan, R.E., Cohen, J.D., 1983. The 1978 National Fire-Danger Rating System: Technical Documentation, USDA Forest Service, Intermountain Forest and Range Experiment Station, General Technical Report INT-169.
Briones-Herrera, C.I., Vega-Nieva, D.J., Monjarás-Vega, N.A., Briseño-Reyes, J., López-Serrano, P.M., Corral-Rivas, J.J., Alvarado-Celestino, E., Arellano-Pérez, S., González, J.G., Ruiz-González, A.D., Jolly, W.M., Parks, S.A., 2020. Near real-time automated early mapping of the perimeter of large forest fires from the aggregation of VIIRS and MODIS active fires in Mexico. Rem. Sens. 12, 1–19.
Brough, A., Gilbertson-Day, J.W., Napoli, J., Scott, J.H., 2020. A fuelscape for all land ownerships in the State of California. <https://pyrologix.com/wp-content/uploads/2021/06/CAL_FuelscapeReport.pdf>.
Canty, A., Ripley, B., 2017. boot: Bootstrap R (S-Plus) functions.
Caprio, A., Swetnam, T.W., 1993. Historic fire regimes along an elevational gradient on the west 457 slope of the Sierra Nevada, California. In: 5th Proceedings: Symposium on 458 Fire in Wilderness and Park Management, Missoula, MT, pp. 173–179.
Carrier, G.F., Fendell, F.E., Feldman, P.S., 1981. Criteria for onset of firestorms. In Hickman, R.G., Meier, C.A., 1983. Proceedings: 17th Asilomar Conference on Fire and Blast Effects of Nuclear Weapons (No. CONF-8305107-). Lawrence Livermore National Lab., CA (USA). pp. 60–65.
Carrier, G.F., Fendell, F.E., Feldman, P.S., 1985. Firestorms. J. Heat Transfer 107, 19–27.
Collins, B.M., Stephens, S.L., 2010. Stand-replacing patches within a mixed severity fire regime: quantitative characterization using recent fires in a long-established natural fire area. Land.e Ecol. 25, 927939.
Coop, J.D., Parks, S.A., Stevens-Rumann, C.S., Crausbay, S.D., Higuera, P.E., Hurteau, M. D., Tepley, A., Whitman, E., Assal, T., Collins, B.M., Davis, K.T., Dobrowski, S., Falk, D.A., Fornwalt, P.J., Fulé, P.Z., Harvey, B.J., Kane, V.R., Littlefield, C.E., Margolis, E.Q., North, M., Parisien, M.A., Prichard, S., Rodman, K.C., 2020. Wildfire-driven forest conversion in western North American landscapes. Bioscience 70, 659–673.
Countryman, C.M., 1964. Mass fires and fire behavior. U. S. Forest Service Research Paper PSW-19, Pacific Southwest Forest and Range Experiment Station, 53 pp.
Di Blasi, C., Branca, C., Santoro, A., Gonzalez Hernandez, E., 2001. Pyrolytic behavior and products of some wood varieties. Combust. Flame 124 (1-2), 165–177.
Dixon, G., Dixon, C., Havis, R., Keyser, C., Rebain, S., Smith-Mateja, E., Vandendriesche, D., 2008. Western Sierra Nevada (WS) Variant Overview – Forest Vegetation Simulator. Internal Rep. Fort Collins, CO: U.S. Department of Agriculture, Forest Service, Forest Management Service Center. 88p.
Dunbar-Irwin, M., Safford, H.D., 2016. Climatic and structural comparison of yellow pine and mixed-conifer forests in northern Baja California (Mexico) and the eastern Sierra Nevada (California, USA). For. Ecol. Manage. 363, 252–266.
Fettig, C.J., Mortenson, L.A., Bulaon, B.M., Foulk, P.B., 2019. Tree mortality following drought in the central and southern Sierra Nevada, California, U.S. For. Ecol. Manage. 432, 164–178. https://doi.org/10.1016/j.foreco.2018.09.006.
Finney, M.A., 1998. FARSITE, Fire Area Simulator–model development and evaluation,. No. 4. US Department of Agriculture Forest Service, Rocky Mountain Research Station.
Finney, M.A., McAllister, S.S., 2011. A review of fire interactions and mass fires. J. Combust. 2011, 1–14.
Finney, M.A., McAllister, S.S., Forthofer, J.M., Grumstrup, T.P., 2021. Wildland Fire Behaviour: Dynamics. CSIRO PUBLISHING, Principles and Processes, p. 360.
Girvetz, E.H., Greco, S.E., 2007. How to define a patch: a spatial model for hierarchically delineating organism-specific habitat patches. Landscape Ecol. 22 (8), 1131–1142.
Goodwin, M.J., Zald, H.S.J., North, M.P., Hurteau, M.D., 2021. Climate-driven tree mortality and fuel aridity increase wildfire's potential heat flux. Geophys. Res. Lett. 48 (24).
Hagmann, R.K., Hessburg, P.F., Prichard, S.J., Povak, N.A., Brown, P.M., Fulé, P.Z., Keane, R.E., Knapp, E.E., Lydersen, J.M., Metlen, K.L., Reilly, M.J., Sánchez Meador, A.J., Stephens, S.L., Stevens, J.T., Taylor, A.H., Yocom, L.L., Battaglia, M.A., Churchill, D.J., Daniels, L.D., Falk, D.A., Henson, P., Johnston, J.D., Krawchuk, M.A., Levine, C.R., Meigs, G.W., Merschel, A.G., North, M.P., Safford, H.D., Swetnam, T. W., Waltz, A.E.M., 2021. Evidence for widespread changes in the structure,

composition, and fire regimes of western North American forests. Ecol. Appl. 31 (8), e02431.
Hessburg, P.F., Prichard, S.J., Hagmann, R.K., Povak, N.A., Lake, F.K., 2021. Wildfire and climate change adaptation of western North American forests: a case for intentional management. Ecol. Appl. 31 (8), e02432.
Huang, S., Ramirez, C., McElhaney, M., Evans, K., 2018. F3: Simulating spatiotemporal forest change from field inventory, remote sensing, growth modeling, and management actions. For. Ecol. Manage. 415–416, 26–37.
Huang, S., Ramirez, C., McElhaney, M., Clark, C., Yao, Z., 2019. Quantifying Spatiotemporal post-disturbance recovery using field inventory, tree growth, and remote sensing. Earth Sp. Sci. 6, 489–504, 10.1029/2018EA000489.
Kane, V.R., Cansler, C.A., Povak, N.A., Kane, J.T., McGaughey, R.J., Lutz, J.A., Churchill, D.J., North, M.P., 2015. Mixed severity fire effects within the Rim fire: relative importance of local climate, fire weather, topography, and forest structure. For. Ecol. Manage. 358, 62–79.
Kilgore, B.M., Taylor, D., 1979. Fire history of a sequoia-mixed conifer forest. Ecol. 60 (129–554), 142.
Knight, C.A., Cogbill, C.V., Potts, M.D., Wanket, J.A., Battles, J.J., 2020. Settlement-era forest structure and composition in the Klamath Mountains: reconstructing a historical baseline. Ecosphere 11 (9), e03250.
Krasnow, K.D., Fry, D.L., Stephens, S.L., 2017. Spatial, temporal and latitudinal components of historical fire regimes in mixed conifer forests. Califor. J. Biogeogr. 44, 1239–1253.
Lareau, N.P., Nauslar, N.J., Bentley, E., Roberts, M., Emmerson, S., Brong, B., Mehle, M., Wallman, J., 2022. Fire-generated tornadic vortices. Bull. Am. Meteorol. Soc.
Lautenberger, C., 2013. Wildland fire modeling with an eulerian level set method and automated calibration. Fire Saf. J. 62, 289–298.
Lautenberger, C., 2017. Mapping areas at elevated risk of large-scale structure loss using monte carlo simulation and wildland fire modeling. Fire Saf. J. 91, 768–775.
Long, J.W., Goode, R.W., Gutteriez, R.J., Lackey, J.L., Anderson, M.K., 2017. Managing California black oak for Tribal ecocultural restoration. J. Forest. 115, 426–434.
Long, J.W., Lake, F.K., Goode, R.W., 2021. The importance of Indigenous cultural burning in forested regions of the Pacific West, USA. For. Ecol. Manage. 500, 119597.
Lydersen, J.M., Collins, B.M., Brooks, M.L., Matchett, J.R., Shive, K.L., Povak, N.A., Kane, V.R., Smith, D.F., 2017. Evidence of fuels management and fire weather influencing fire severity in an extreme fire event. Ecol. Appl. 27 (7), 2013–2030.
Lydersen, J.M., Collins, B.M., Coppoletta, M., Jaffe, M.R., Northrop, H., Stephens, S.L., 2019. Fuel dynamics and reburn severity following high-severity fire in a Sierra Nevada, USA, mixed-conifer forest. Fire Ecol. 15 (1), 1–14.
Lydersen, J.M., North, M.P., Collins, B.M., 2014. Severity of an uncharacteristically large wildfire, the Rim Fire, in forests with relatively restored frequent fire regimes. For. Ecol. Manage. 328, 326–334.
Miller, J.D., Thode, A.E., 2007. Quantifying burn severity in a heterogeneous landscape with a relative version of the delta Normalized Burn Ratio (dNBR). Remote Sens. Environ. 109, 66–80.
Miller, J.D., Safford, H.D., Crimmins, M., Thode, A.E., 2009. Quantitative evidence for increasing forest fire severity in the Sierra Nevada and Southern Cascade Mountains, California and Nevada, USA. Ecosystems 12, 16–32.
Miller, J.D., 2017. R5: VegBurnSeverityBA edition 18_1. USDA Forest Service, Pacific Southwest Region, Fire and Aviation Management. [dataset].
Minnich, R.A., Barbour, M.G., Burk, J.H., Fernau, R.F., 1995. Sixty years of change in Californian conifer forests of the San Bernardino Mountains. Conserv. Biol. 9, 902–914.
Minnich, R.A., Goforth, B.R., Paine, T.D., 2016. Follow the water: extreme drought and the conifer forest pandemic of 2002–2003 along the California borderland. In: Paine, T.D., Lieutier, F. (Eds.), Insects and Diseases of Mediterranean Forest Systems. Springer International Publishing, Switzerland, pp. 859–890.
Murphy, J.S., York, R., Rivera Huerta, H., Stephens, S.L. 2021. Characteristics and metrics of resilient forests in the Sierra de San Pedro Martír, Mexico. For. Ecol. Manage. 482, 118864.
National Interagency Fire Center. 2020. <https://ftp.wildfire.gov/public/incident_specific_data/calif_s/!2020_Incidents/CA-SNF-001391_Creek/IR/NIROPS/>.
National Oceanic and Atmospheric Administration, 2020. <https://www.nco.ncep.noaa.gov/pmb/products/rtma/>.
National Wildfire Coordinating Group, 2020a. <https://inciweb.nwcg.gov/incident/7147/>.
National Wildfire Coordinating Group, 2020b. <https://fsapps.nwcg.gov/afm/data/fireptdata/modis_fire_2020_366_conus_shapefile.zip>.
National Wildfire Coordinating Group, 2020c. <https://fsapps.nwcg.gov/afm/data_viirs_iband/fireptdata/viirs_iband_fire_2020_366_conus_shapefile.zip>.
Nelson Jr, R.M., 2003. Reaction times and burning rates for wind tunnel headfires. Int. J. Wildland Fire 12, 195–211.
NIFC, 2020. National Large Incident Year-to-Date Report. <https://gacc.nifc.gov/sacc/predictive/intelligence/NationalLargeIncidentYTDReport.pdf>.
North, M., Collins, B.M., Stephens, S., 2012. Using fire to increase the scale, benefits, and future maintenance of fuels treatments. J. For. 110 (7), 392–401.
North, M.P., York, R.A., Collins, B.M., Hurteau, M.D., Jones, G.M., Knapp, E.E., Kobziar, L., McCann, H., Meyer, M.D., Stephens, S.L. Tompkins, R.E., 2021. Pyrosilviculture needed for landscape resilience of dry western United States forests. J. For. 119, 520–544.
North, M.P., Tompkins, R.E., Bernal, A.A., Collins, B.M., Stephens, S.L., York, R.A. 2022. Operational resilience in western US frequent-fire forests. For. Ecol. Manage. 507, 120004.
Parks, S.A., Holsinger, L.M., Voss, M.A., Loehman, R.A., Robinson, N.P., 2018. Mean composite fire severity metrics computed with google earth engine offer improved accuracy and expanded mapping potential. Rem. Sens. 10, 1–15.
Peterson, D.A., Hyer, E.J., Campbell, J.R., Solbrig, J.E., Fromm, M.D., 2017. A conceptual model for development of intense pyrocumulonimbus in western North America. Mon. Weather Rev. 145 (6), 2235–2255.
Pitts, W.M., 1991. Wind effects on fires. Prog. Energy Combust. Sci. 17, 83–134.
Pebesma, E., 2018. Simple features for R: Standardized support for spatial vector data. R J. 10.1, 439–446. <https://doi.org/10.32614/RJ-2018-009>.
Povak, N.A., Kane, V.R., Collins, B.M., Lydersen, J.M., Kane, J.T., 2020. Multi-scaled drivers of severity patterns vary across land ownerships for the 2013 Rim Fire, California. Land. Ecol. 35, 293–318.
Prichard, S.J., Hessburg, P.F., Hagmann, R.K., Povak, N.A., Dobrowski, S.Z., Hurteau, M. D., Kane, V.R., Keane, R.E., Kobziar, L.N., Kolden, C.A., North, M., Parks, S.A., Safford, H.D., Stevens, J.T., Yocom, L.L., Churchill, D.J., Gray, R.W., Huffman, D.W., Lake, F.K., Khatri-Chhetri, P., 2021. Adapting western North American forests to climate change and wildfires: 10 common questions. Ecol. Appl. 31 (8).
Rivera-Huerta, H., Safford, H.D., Miller, J.D., 2016. Patterns and trends in burned area and fire severity from 1984 to 2010 in the Sierra de San Pedro Martir, Baja California. Mexico. Fire Ecol. 12, 52–72.
Rothermel, R.C. 1972. A mathematical model for predicting fire spread in wildland fuels. USDA For. Serv. Res. Pap. INT-115.
Safford, H.D., Stevens, J.T., 2017. Natural range of variation for yellow pine and mixed-conifer forests in the Sierra Nevada, southern Cascades, and Modoc and Inyo National Forests, California, USA. General Technical Report PSWGTR-256. U.S. Department of Agriculture, Forest Service, Pacific Southwest Research Station, Albany, California, USA.
Safford, H.D., Paulson, A.K., Steel, Z.L., Young, D.J.N., Wayman, R.W., 2022. The 2020 California fire season: a year like no other, a return to the past or a harbinger of the future? Glob. Ecol. Biogeogr. in press.
Sanchez, M.A., 2019. patchwoRk: patch delineation package. <https://github.com/bi0m3trics/patchwoRk>.
Sims, T., 2004. Dead tree count totals in 2004. San Bernardino and San Jacinto Mountains Vegetation Mortality Project, San Bernardino National Forest, CALMAST, and ESRI, Redlands, CA.
Sánchez Meador, A, 2019. patchwoRk: Patch Delineation Package. R package version 1.0.0. https://github.com/bi0m3trics/patchwoRk.
Stephens, S.L., 2004. Fuel loads, snag density, and snag recruitment in an unmanaged Jeffrey pine-mixed conifer forest in northwestern Mexico. For. Ecol. Manage. 199, 103–113.
Stephens, S.L., Skinner, C.N., Gill, S.J., 2003. Dendrochronology-based fire history of Jeffrey pine-mixed conifer forests in the Sierra San Pedro Martir. Mexico. Can. J. For. Res. 33 (6), 1090–1101.
Stephens, S.L., Fule, P.Z., 2005. Western pine forests with continuing frequent fire regimes: possible reference sites for management. J. For. 103, 357–362.
Stephens, S.L., Gill, S.J., 2005. Forest structure and mortality in an old-growth Jeffrey pine-mixed conifer forest in northwestern Mexico. For. Ecol. Manage. 205 (1-3), 15–28.
Stephens, S.L., Moghaddas, J.J., Ediminster, C., Fiedler, C.E., Hasse, S., Harrington, M., Keeley, J.E., McIver, J.D., Metlen, K., Skinner, C.N., Youngblood, A., 2009. Fire treatment effects on vegetation structure, fuels, and potential fire severity in western U.S. forests. Ecol. Appl. 19, 305–320.
Stephens, S.L., Lydersen, J.M., Collins, B.M., Fry, D.L., Meyer, M.D., 2015. Historical and current landscape-scale ponderosa pine and mixed-conifer forest structure in the Southern Sierra Nevada. Ecosphere 6 (5), art 79.
Stephens, S.L., Collins, B.M., Fettig, C.J., Finney, M.A., Hoffman, C.M., Knapp, E.E., North, M.P., Safford, H., Wayman, R.B., 2018. Drought, tree mortality, and wildfire in forests adapted to frequent fire. Bioscience 68, 77–88.
Stephens, S.L., Battaglia, M.A., Churchill, D.J., Collins, B.M., Coppoletta, M., Hoffman, C. M., Lydersen, J.M., North, M.P., Parsons, R.A., Ritter, S.M., Stevens, J.T., 2021. Forest restoration and fuels reduction: Convergent or divergent? Bioscience 71, 85–101.
Stevens, J.T., Collins, B.M., Miller, J.D., North, M.P., Stephens, S.L., 2017. Changing spatial patterns of stand-replacing fire in California mixed-conifer forests. For. Ecol. Manage. 406, 28–36.
Stevens, J.T., Lydersen, J.M., Collins, B.M., 2021. Postfire Restoration Framework for National Forests in California Appendix 4: Burn Severity Spatial Analyses. Meyer, M. D., Long, J.W., Safford, H.D. (Eds.). General Technical Report PSW-GRT-270. pp. 175–182.
Therneau, T., Atkinson, B., 2019. rpart: Recursive partitioning and regression trees. <https://cran.r-project.org/package=rpart>.
United States Department of Agriculture National Agriculture Imagery Program. NAIP 2020 Natural Color, California. California Department of Fish and Wildlife [image].
United States Forest Service, 2020. <https://www.wfas.net/index.php/national-fuel-moisture-database-moisture-drought-103>.
Waigl, C.F., Stuefer, M., Prakash, A., Ichoku, C., 2017. Detecting high and low-intensity fires in Alaska using VIIRS I-band data: an improved operational approach for high latitudes. Rem. Sens. Environ. 199, 389–400.
Westerling, A.L., 2016. Increasing western US forest wildfire activity: sensitivity to changes in the timing of spring. Philos. Trans. Roy. Soc. B 371, 20150178.
Williams, A.P., Cook, B.I., Smerdon, J.E., 2022. Rapid intensification of the emerging southwestern North American megadrought in 2020–2021. Nat. Clim. Change 12 (3), 232–234.